Monolayer Pattern Evolution via Substrate Strain-Mediated Spinodal Decomposition

Kevin S. Schneider,[1] Wei Lu,[2] Thomas M. Owens,[1] Daniel R. Fosnacht,[1] M. M. Banaszak Holl,[1,4] and B. G. Orr[3,4]

[1]*Chemistry Department, The University of Michigan, Ann Arbor, Michigan 48109-1055, USA*
[2]*Mechanical Engineering Department, The University of Michigan, Ann Arbor, Michigan 48109-2125, USA*
[3]*Physics Department, The Harrison M. Randall Laboratory, The University of Michigan, Ann Arbor, Michigan 48109-1120, USA*
[4]*Applied Physics Program, The Harrison M. Randall Laboratory, The University of Michigan, Ann Arbor, Michigan 48109-1120, USA*

(Received 25 July 2003; published 15 October 2004)

Investigations of octylsilane ($C_8H_{17}SiH_3$) monolayer pattern formation on Au(111) are reported. Scanning tunneling microscopy data display the evolution of a ~6 nm scale pattern of interwoven features concomitant with ejection of surface Au atoms and relaxation of the Au(111) $23 \times \sqrt{3}$ surface reconstruction. Numerical simulations suggest the surface dynamics are governed by a substrate strain-mediated spinodal decomposition mechanism, novel to organic monolayer formation. Collectively, the experimental and theoretical data indicate strain-inducing Si-Au bond interactions drive the pattern formation and the alkyl chains play a negligible role.

DOI: 10.1103/PhysRevLett.93.166104 PACS numbers: 68.35.–p, 68.37.Ef, 68.43.Jk

In this Letter, we report the first observation of substrate strain-mediated spinodal decomposition to produce nanoscale patterning of a chemisorbed organic monolayer. Although strain is frequently found to drive self-assembly in numerous thin film material systems, [1–3] these findings are unique to the field of self-assembled monolayers (SAMs) on solid substrates. The general significance of the observations includes the length scale and physical pattern formation mechanism, both of which differ dramatically from alkanethiol SAM systems where evolving monolayer features are commonly attributed to alkyl chain-chain interactions [4–7].

Recently, the formation of chemisorbed alkylsilane monolayers on Au(111) was demonstrated [8]. Reflection-adsorption infrared and x-ray photoelectron spectroscopic (XPS) studies indicate alkylsilane adsorption occurs via scission of the three Si-H bonds and covalent bonding of the Si head group to the Au surface. The narrow width of the Si $2p$ features in XPS spectra indicate the Si atoms are in a chemically homogenous environment and is consistent with formation of a chemisorbed monolayer at room temperature [8]. In addition, spectroscopic data indicate the alkyl chains are intact within the chemisorbed monolayer. Adsorption rapidly occurs with 75% surface coverage achieved by 5 L (L = 1×10^{-6} torr s) exposure (Fig. 1). Afterwards, adsorption dynamics slow dramatically with saturation coverage reached at 300 L exposure. Comparison with alkanethiol adsorption indicates $95 \pm 5\%$ monolayer surface coverage [9]. Here, scanning tunneling microscopy (STM) is employed to investigate pattern formation dynamics of the *n*-octylsilane ($C_8H_{17}SiH_3$) monolayer. The central goal of these studies is to elucidate the pattern formation mechanism of the complex nanoscale structures exhibited by the octylsilane monolayer (Fig. 2).

The chemisorbed monolayer is synthesized by gaseous dosing of octylsilane onto a freshly evaporated Au(111) surface in ultrahigh vacuum (UHV) conditions ($\leq 3 \times 10^{-10}$ torr). Typical dosing pressures are $\sim 10^{-7}$ torr with a substrate temperature of ~300 K. STM studies are performed in two manners: exposing the substrate to gaseous octylsilane in a separate dosing chamber or dosing directly into the STM chamber while the tip is retracted ~100 nm during exposure to the adsorbate flux. Both techniques yield identical results; however, the second method requires slightly higher octylsilane exposures to achieve saturation coverage (due to a shielding effect from the STM tip). Commercial Pt-Ir tips are employed for tunneling. High gap impedance (GΩ) tunneling (0.1 nA and ±1.0 V) is employed to ensure nonperturbative experimental conditions.

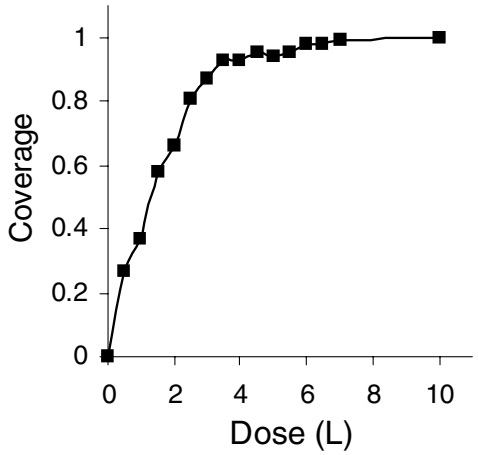

FIG. 1. Normalized XPS carbon 1*s* core level intensity *versus* dose. The reference value for complete coverage was a 300 L dose. The data indicate 75% octylsilane surface coverage on Au(111) at 5 L octylsilane exposure.

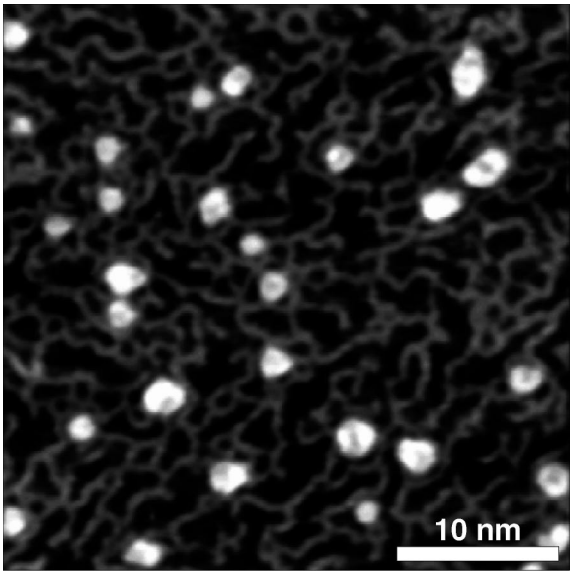

FIG. 2. A 35×35 nm UHV-STM image of the monolayer formed from exposure of Au(111) to 50 L gaseous octylsilane; $V_S = -1.00$, $I_T = 0.26$ nA.

Sequential STM images acquired as a function of increasing octylsilane exposure are displayed in Fig. 3. The striped pattern of the Au(111) $23 \times \sqrt{3}$ surface reconstruction is faintly visible running diagonally in Fig. 3(a). Following 2 L octylsilane exposure, the surface appears unchanged [Fig. 3(b)]. However, the appearance of darkly contrasted ~0.08 nm surface depressions is apparent following 5 L total octylsilane exposure [Fig. 3(c)].

Increasing the total octylsilane exposure from 5–11 L, increases both the quantity and size of the surface depressions [Figs. 3(d)–3(f)]. STM images of the substrate surface following 20, 32, and 45 L octylsilane exposures are displayed in Figs. 3(g)–3(i). Several important features appearing during evolution of the terminal monolayer structure warrant discussion: (1) emergence of a characteristic two-phase nanoscale pattern, (2) relaxation of the Au(111) $23 \times \sqrt{3}$ surface reconstruction, and (3) nucleation of Au islands and growth of substrate terrace edges.

Evolution of the monolayer surface pattern from an initial array of darkly contrasted surface depressions to a complex pattern of interwoven sinuous ridges is evident in Fig. 3. Increasing octylsilane exposure yields additional surface depressions and enlarges preexisting depressions to ultimately develop a ~6 nm characteristic size. In addition, a new "light" phase—the interwoven sinuous ridges—emerges at the boundaries of the dark regions.

Relaxation of the Au(111) $23 \times \sqrt{3}$ surface reconstruction results in ejection of the excess surface Au atoms. The Au(111) $23 \times \sqrt{3}$ surface is uniaxially compressed by ~4.3% [10]. This source of Au adatoms provides a

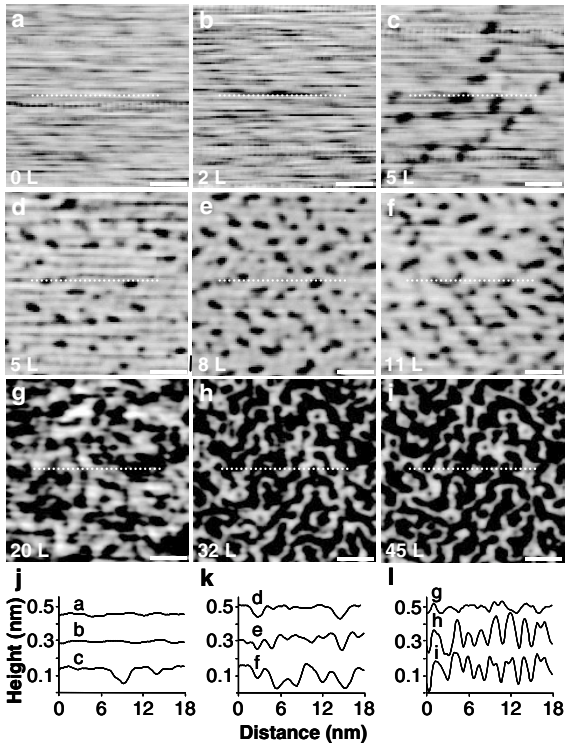

FIG. 3. Incremental *in situ* UHV-STM images of Au(111) as a function of increasing octylsilane exposure (langmuirs, L, indicated in the lower left corner). Panels (a)–(c), (d)–(f), and (g)–(i) monitor sequential substrate changes of three separate sample regions. All images are 25×25 nm in area and were acquired at $V_S = -1$ V and $I_T = 7$–30 pA. The scale bar in the bottom right corner of each image indicates 5 nm. Panels (j)–(l) display the cross-sectional profiles denoted by the dashed lines in the corresponding images.

partial explanation for the growth of the Au islands apparent in Fig. 2. The apparent heights (~2.5 Å) of the Au islands are identical to the monoatomic step height of a Au(111) terrace. The sinuous monolayer pattern on a terrace traverses the Au islands and continues on without disruption, suggesting the islands nucleate underneath the chemisorbed monolayer and effectively lift it up one atomic layer. Quantitative analysis of the terminal monolayer features indicates the Au islands nucleate over ~7–10% of the surface whereas the dark and light monolayer phases are present in nearly equivalent amounts.

Occasionally, individual mobile Au adatoms having apparent heights of ~1.5 Å temporarily appear [11]. The mobile Au adatoms are observed at octylsilane exposures prior to Au island nucleation. The adatoms either subsequently disappear or become static and enlarge into Au islands. However, adatom diffusion is quite rapid and precludes extensive tracking. A second dynamic event entails rearrangement of the two (dark and light) monolayer phases. The changes are local, reversible, and subtle. Close inspection of the STM data reveals adjacent sinu-

ous ridges combining, breaking and/or exhibiting lateral "switching" behavior.

The octylsilane monolayer pattern lacks the atomic scale features frequently observed in alkanethiol SAMs and is instead reminiscent of mesostructures formed by magnetic phases [12], block copolymers [13], and metal alloys [14]. The island coverage (7–12% lower bound) indicates approximately 2 to 3 times as many Au adatoms are ejected from the surface layer than is normally expected from simple relaxation of the Au(111) $23 \times \sqrt{3}$ surface reconstruction (~4.3%). Therefore, a mechanism involving ejection of additional Au atoms from the surface layer is likely.

Similar island quantities have also been observed during alkanethiol SAM formation [11]. A recent density functional theory (DFT) study has identified the formation of an ordered defect vacancy phase on Au(111) as providing an additional source of Au adatoms during alkanethiol SAM formation [15]. Furthermore, the DFT calculations indicate the vacancy phase is lower in energy when the surface adsorbate coverage is sufficiently high to induce interaction between multiple surface vacancies. Physically, this interaction arises when the energy gained from elastic relaxation of the substrate is greater than the energy required to break the bonds associated with atom ejection. The DFT calculations indicate the adsorbate-induced surface vacancy reconstruction is independent of specific adsorbate bonding sites and is instead contingent upon the gross reduction in substrate strain energy [15]. This hypothesis is supported by recent experimental investigations of alkanethiol SAM formation on Cu(111) in which adsorbate-induced surface vacancy reconstructions have also been observed [16].

Consideration of the aforementioned theoretical and experimental work suggests the darkly contrasted surface depressions apparent at low octylsilane exposures [Figs. 3(c)–3(f)] correspond to regions of adsorbate-induced surface vacancies. Preliminary molecular mechanics and quantum chemical calculations suggest the Au atom directly beneath an adsorbed octylsilane molecule is preferentially ejected. The calculations indicate creation of the adsorbate-induced surface vacancy site significantly reduces the molecular adsorption energy and relaxes the Si head group towards the surface.

Recall the XPS data indicate 75% surface coverage at 5 L octylsilane exposure (Fig. 1), whereas the STM data first show the appearance of small depressed regions following 5 L exposure. However, the lack of STM image contrast information does not necessarily rule out additional molecular adsorption. Evidence for adsorption is instead found in area-averaged tunnel junction scanning tunneling spectroscopy (STS) data which confirm 75% surface coverage at 5 L octylsilane exposure [17].

Collectively, the STM, XPS, and STS data indicate the presence of two molecular adsorption phases within the chemisorbed octylsilane monolayer. The dark phase corresponds to regions of molecular adsorption in adsorbate-induced surface vacancy sites, whereas the light phase (constituting the sinuous ridge features) corresponds to molecular chemisorption in regions devoid of surface vacancies.

We now consider the phase segregation and resulting monolayer pattern formation mechanisms. A primary difference between the two molecular adsorption phases entails the presence of Au surface vacancies, which reasonably implies an elastic substrate interaction between the two phases. To investigate the potential role of substrate interaction in the monolayer pattern formation mechanism, a model for substrate strain-mediated phase separation via spinodal decomposition has been developed. The numerical model discussed herein is a direct extension of previously developed methods [18]. Fundamentally, the model starts from a free energy that includes positive terms arising from the phase boundary and elastic deformation of the substrate. The boundary energy is lowered by reducing the interface length (i.e., domain coarsening), whereas the elastic energy is reduced by refining the domain size to reduce the fringing elastic deformation of the substrate. Minimization of the free energy produces a competition between these effects and yields a model containing two fundamental length scales: $l \equiv$ the domain feature size and $b \equiv$ the scale of the transition region between the two monolayer phases. Utilizing parameters for the Young's modulus ($\sim 10^{11}$ N/m^2) and bonding energy (~1 eV) appropriate for the Au/octylsilane system, the length scales are calculated to be $l \approx 6$ nm and $b \approx 0.6$ nm. Revisiting the terminal monolayer structures displayed in Fig. 2 reveals the domain size l agrees well with the ~6 nm estimate from the computational model. In addi-

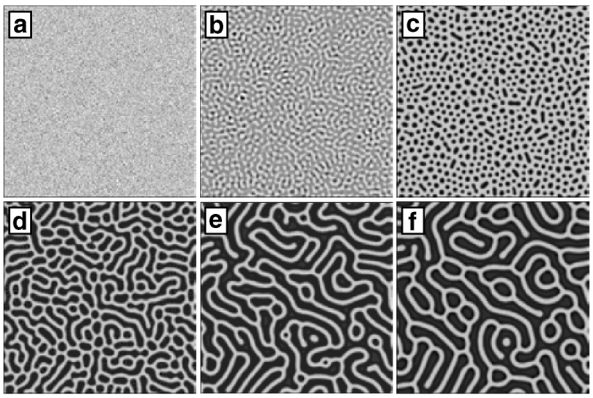

FIG. 4. Theoretical simulation investigating the self-assembly and pattern formation dynamics of a two-phase monolayer on a solid substrate. The percentage of the dark phase increases from 40% in (a) to a fixed 60% concentration in (d). Figures (e) and (f) highlight additional feature coarsening over time where the normalized simulation times are (a) $\tau = 0$, (b) $\tau = 10$, (c) $\tau = 90$, (d) $\tau = 400$, (e) $\tau = 1000$, and (f) $\tau = 90\,000$. The length scale of the resulting pattern in (f) is 6 nm.

tion, the transition region between phases *b* is quite abrupt (i.e., atomic in scale). With the proper length scales predicted via the model, it is further instructive to compare the temporal evolution of the model dynamics with the experimental STM data displayed in Fig. 3.

A sequence of images (Fig. 4) obtained from numerical integration of the isotropic 2D model displays evolution of a complex pattern as the concentration of the finely dispersed dark phase (40% initial concentration) is increased relative to the light phase over time. By dynamically changing the phase concentrations, the simulation mimics the STM data, which indicate increasing quantities of the dark phase concurrent with increasing octylsilane adsorption. In the simulation, the concentration of the dark phase is increased to 60% [Fig. 4(d)] and the surface coarsens under the model dynamics for minimization of the free energy.

In both the experimental and theoretical images, the dark phase first nucleates as isolated regions [Figs. 3(c) and 4(c)]. Expansion and interaction of these regions yields an interwoven pattern [Figs. 3(g) and 4(d)]. Finally, the features coarsen to a steady-state length scale to generate a constant pattern. (Note, the computational model does not incorporate nucleation of the Au islands.) An important difference between the substrate elastically mediated spinodal decomposition model and the conventional spinodal model [19] involves the saturation of feature coarsening. In the conventional model, feature sizes grow as $t^{1/3}$; however, inclusion of substrate elastic interaction produces an asymptotic length scale l for the pattern features. Unfortunately, it is difficult to experimentally distinguish slow coarsening from a constant value, although the sizes of the experimental monolayer surface structures are invariant over the course of several days.

Consideration of the experimental and theoretical data produces a detailed picture of the monolayer surface dynamics. Low-coverage (<5 L) octylsilane adsorption rapidly occurs without substrate vacancy formation. Continued octylsilane exposure increases molecular adsorbate density until it is energetically favorable to nucleate a vacancy defect phase on the Au(111) surface. At this stage, adsorption rate dramatically decreases and surface vacancy formation via ejection of Au surface atoms provides a source of Au adatoms. Increasing octylsilane chemisorption yields localized domains of vacancy phase regions that continue to nucleate and ripen while Au adatoms diffuse to substrate terraces, resulting in Au terrace growth underneath the chemisorbed layer. In addition, subtle and dynamic rearrangements of the two molecular adsorption phases further reduce the total free-energy of the system. The combination of surface dynamics yields the complex sinuous pattern displayed by the terminal monolayer surface. In the final stages, the pattern coarsens and the mobility of the Au adatoms decreases (likely due to the increased adsorbate density) resulting in agglomeration of Au islands underneath the chemisorbed octlysilane monolayer.

In conclusion, STM has been employed to examine the nanoscale pattern formation dynamics of *n*-octylsilane ($C_8H_{17}SiH_3$) on Au(111). Exposure of Au(111) to gaseous octylsilane in UHV yields two molecular adsorption phases. Segregation of the two adsorption phases within the chemisorbed monolayer via a substrate strain-mediated spinodal decomposition mechanism yields a surface pattern containing a characteristic $\sim$6 nm feature size. In contrast to analogous alkanethiol SAMs, alkyl chain-chain interactions do not play a significant role in the surface ordering. Numerical simulations of the surface dynamics display good agreement with the experimental data both in terms of the spatial scale and temporal evolution.

Support for this work was provided by the NSF (DMR-0093641) and RHK Technology, Inc. D. R. F. thanks the NSF for financial support (DGE-9972776). Y. Chen is thanked for numerous helpful discussions.

[1] C. W. Snyder, B. G. Orr, D. Kessler *et al.*, Phys. Rev. Lett. **66**, 3032 (1991).
[2] F. Liu, Phys. Rev. Lett. **89**, 246105 (2002).
[3] S. R. Shinde, A. S. Ogale, S. B. Ogale *et al.*, Phys. Rev. B **64**, 035408 (2001).
[4] A. Ulman, Chem. Rev. (Washington, D.C.) **96**, 1533 (1996).
[5] G. E. Poirier and E. D. Pylant, Science **272**, 1145 (1996).
[6] G. E. Poirier, Chem. Rev. **97**, 1117 (1997).
[7] Z. J. Donhauser, B. A. Mantooth, K. F. Kelly *et al.*, Science **292**, 2303 (2001).
[8] T. M. Owens, K. T. Nicholson, M. M. Banaszak Holl *et al.*, J. Am. Chem. Soc. **124**, 6800 (2002).
[9] T. M. Owens, S. Suzer, and M. M. Banaszak Holl, J. Phys. Chem. B **107**, 3177 (2003).
[10] U. Harten, A. M. Lahee, J. P. Toennies *et al.*, Phys. Rev. Lett. **54**, 2619 (1985).
[11] G. E. Poirier, Langmuir **13**, 2019 (1997).
[12] E. A. Giess, Science **208**, 938 (1980).
[13] M. Park, C. Harrison, P. M. Chaikin *et al.*, Science **276**, 1401 (1997).
[14] R. Plass, J. A. Last, N. C. Bartelt *et al.*, Nature (London) **412**, 875 (2001).
[15] L. M. Molina and B. Hammer, Chem. Phys. Lett. **360**, 264 (2002).
[16] S. M. Driver and D. P. Woodruff, Langmuir **16**, 6693 (2000).
[17] K. S. Schneider, W. Lu, D. R. Fosnacht *et al.*, Langmuir **20**, 1258 (2004).
[18] W. Lu and Z. Suo, Phys. Rev. B **65**, 205418 (2002).
[19] J. W. Cahn and J. E. Hilliard, J. Chem. Phys. **28**, 258 (1958).